RSC Advances

PAPER

View Article Online
View Journal | View Issue

Cite this: *RSC Adv.*, 2023, **13**, 8736

Electro-oxidation reconstitution of aluminium copper MOF-derived metal oxyhydroxides for a robust OER process

H. A. Alburaih,[a] Sumaira Manzoor,[b] M. Abdullah,[c] M. N. Ashiq,[b] Salma Aman,[b] Sergei V. Trukhanov,[de] Tatiana I. Zubar,[*e] Zhipeng Sun,[f] T. A. Taha[gh] and Alex V. Trukhanov[de]

It is common knowledge that the O_2 evolution reaction (OER) is a crucial half-reaction in the electrolysis of water. However, it is currently difficult to create inexpensive OER electrode materials in a way that is efficient, simple, and environmentally friendly. In this research, metal oxy-hydroxides with numerous oxygen defects (M-OOHv) are created at surface of Cu foam (CF) using a unique, straightforward electro-oxidation reconstitution (ER) process. Different spectroscopic and microscopy methods are used to analyse the electrode characteristics of Al_2Cu-MOF@M-OOHv-ER/CF; electrochemical measurements display a lower overpotential (η) of 366 mV @ 10 mA cm^{-2} and a Tafel slope of 95.2 mV dec^{-1} in 1.0 M KOH. X-Ray diffraction (XRD), scanning electron microscopy (SEM), and Raman studies confirm the phase transition of the metal–organic framework (MOF) to the M-OOH, which acts as the active site to boost the OER activity. Through spectroscopic and microscopic investigations, it is determined that the efficiency of bimetallic electrode materials and oxygen vacancies in the M-OOHv have an impact on the electron power density. The manufactured electrode material additionally showed good durability for 50 hours. As a result, the newly developed Al_2Cu-MOF@M-OOHv-ER/CF nanomaterial has greater potential for both electrolysis of water and other energy storage equipment.

Received 1st December 2022
Accepted 30th January 2023

DOI: 10.1039/d2ra07661f

rsc.li/rsc-advances

1 Introduction

The requirement for clean, nondepletable energy reservoirs is a hot topic because of the current energy crisis. Functional materials for distinctly efficient hydrogen evolution reactions (HER) and oxygen evolution reactions (OER) attract considerable attention.[1–6] A highly active electrode material for the OER is urgently required because the OER has a sluggish kinetics as compared to the HER. Due to excellent oxygen evolution electrocatalytic performance, contemporary IrO_2 and RuO_2, *etc.* are valuable metals for electrocatalysts. However IrO_2 and RuO_2 are not frequently employed in actual commercial applications because of their small reserves, high cost, and unstable nature.[7–11] There is a lot of interest in transition metal-based materials (TMMs) as alternatives to precious metal-based materials because they have enormous reserves and various electronic structures that make them appropriate for binding to intermediates.[12–14] Metal oxides (MOs), metal hydroxides (MOHs), and metal oxy-hydroxides (MOOHs) are a few of the compounds that have a major impact on the success of the fundamental O_2 evolution process. Directly produced TMMs are insufficient because the OER requires a large surface area and a certain shape to expose more active sites.[15–19]

Therefore, metal–organic frameworks (MOFs) have regarded as electrocatalysts for OER due to their improved specific surface area as well as periodic structure.[20] It is tough to further boost the electrocatalytic performance of MOFs on account of their poor electrical conductivity and catalytic activity.[20–22] Calcination at high temperatures can convert MOFs with high catalytic activity to the metal oxides. In addition, the presence of a carbon layer can improve the electrical conductivity.[23–25] While high-temperature calcination can increase the conductivity and introduce more catalytically active sites, it is also very energy-intensive, waste-producing, and impure.[26–28] This makes it

[a]*Department of Physics, College of Science, Princess Nourah bint Abdulrahman University, P.O. Box 84428, Riyadh 11671, Saudi Arabia*
[b]*Institute of Chemical Sciences, Bahauddin Zakariya University, Multan 60800, Pakistan*
[c]*Department of Chemistry, Government College University, Lahore, Pakistan*
[d]*Smart Sensors Laboratory, Department of Electronic Materials Technology, National University of Science and Technology MISiS, Moscow 119049, Russia*
[e]*Scientific-Practical Materials Research Centre of National Academy of Sciences of Belarus, Minsk 220072, Belarus. E-mail: fix.tatyana@gmail.com*
[f]*School of Materials and Energy, Guangdong University of Technology, Guangzhou Higher Education Mega Center, No.100 Waihuan Xi Road, Panyu District, Guangzhou 510006, P. R. China*
[g]*Physics Department, College of Science, Jouf University, P.O. Box 2014, Sakaka, Saudi Arabia*
[h]*Physics and Engineering Mathematics Department, Faculty of Electronic Engineering, Menoufia University, Menouf 32952, Egypt*

necessary to find out an effective, uncomplicated, and ecologically friendly technique to create electrocatalysts that perform wonderfully, which is still an obstacle. However, it has been shown that M-OOHs exhibit outstanding OER electrocatalytic efficacy and developing the corresponding M-OOHv from MOFs with high specific surface area will considerably enhance OER efficiency.[29,30] Furthermore, scientists studied the bimetallic MOF, such as Ling *et al.*, who synthesized the $Fe_{0.67}Co_{0.33}OOH$ on nickel foam for OER activity. The electrocatalytic result of $Fe_{0.67}Co_{0.33}OOH$ displays 45.3 mV dec^{-1} and a Tafel slope of 244 mV @ 10 mA cm^{-2}.[31] Frang *et al.* developed the defect rich (Co, Fe)$_3O_4$ for the OER process. Current density at 10 mA cm^{-2} alongside Tafel slope around 41 mV dec^{-1}, the electrochemical performance related to (Co, Fe)$_3O_4$ indicated a smaller overpotential of 286 mV. Due to the enhanced electrochemical result, the enrichment of active centers and defective species occurred.[32]

In the present study, an Al_2Cu-MOF@M-OOHv-ER/CF nanomaterial is developed by an electro-oxidation reconstitution procedure from an Al/Cu bimetallic organic framework (Al_2CuMOF) on copper foam, resulting in a metal hydroxide with copious oxygen vacancies (M-OOHv) on the interface of Al_2Cu-MOF/CF. The substrate, which is copper foam, has a high porosity and improves the conductivity in addition to exposing a lot of active centers. Additionally, the efficacy of O_2 evolution is greatly enhanced when oxygen defect engineering is used in conjunction with the M-OOH. Due to the formation of defects in the crystal structure, the way the electrons are organized can change. This improves the conductivity and accelerates the adsorption of water molecules. With a morphology similar to saw-toothed edges, Al_2Cu-MOF@M-OOHv-ER/NF manifests huge electrochemically active surface area (ECSA), a BET surface area of 173 m^2 g^{-1}, and stable long-term operation without decay for 50 hours at 1.77 V. Its overpotential is just 366 mV measured @ 10 mA cm^{-1}. The MOF to M-OOHv phase change seen by *in situ* Raman indicates oxygen defects. In addition, many analytical methods were used to quantify the structural modifications that prove oxygen defects in the MOOHv and the bimetal synergistic effect, which regulate the electron density of states, and are responsible for the enhanced OER catalytic activity. Furthermore, the newly developed Al_2Cu-MOF@M-OOHv-ER/CF nanomaterial has vast application capability for complete water splitting and can be produced in an effective, straightforward, and environmentally friendly way and has significant oxygen evolution performance.

2 Experimental

2.1. Chemicals and reagents

Aluminum nitrate ($Al(NO_3)_3\cdot 9H_2O$, ≥98%), copper(II) nitrate ($Cu(NO_3)_2\cdot 3H_2O$, 99%), terephthalic acid ($C_8H_6O_4$, H_2BDC), *N*,*N*-dimethylformamide (C_3H_7NO, DMF), absolute ethanol (C_2H_6O, 95.0%), and kalium hydroxide (KOH, ≥85%), all were obtained from Sigma-Aldrich. There was no need to purify the aforementioned chemical reagents because they were all of analytical grade.

2.2. Synthesis of Al_2Cu-MOF/CF

First, to get rid of any surface impurities, the CF (1 cm × 1 cm) was ultrasonically treated for 10 min in 1.0 M HCl, CH_3CH_2OH, and DI water. The precursors used for the fabrication of Al_2Cu-MOF/CF were $Cu(NO_3)_2\cdot 3H_2O$ (160 mg, 0.5 mmol), terephthalic acid (265 mg, 1.65 mmol), and $Al(NO_3)_3\cdot 9H_2O$ (280 mg, 1.1 mmol). All these precursors were then disintegrated in mixture of 50 mL DMF, 5 mL of CH_3CH_2OH, along with 5 mL of DI H_2O. Consequently, this uniform mixture was then shifted to a 100 mL hydrothermal reactor along with the already cleaned CF and then placed in the electric furnace for six hours at 160 °C. The autoclave was then allowed to cool at ambient temperature. Then the fabricated Al_2Cu-MOF/CF was repeatedly washed with absolute ethanol and double distilled H_2O to eliminate any remaining organic ligands after the hydrothermal process. At 60 °C for 6 hours, the newly synthesized bimetallic Al_2Cu-MOF/CF was then dried, and stored for further characterization.

2.3. Synthesis of Al_2Cu-MOF@M-OOHv-ER/CF

For the fabrication of Al_2Cu-MOF@M-OOHv-ER/CF, the electrochemical method was used. For this purpose, the synthesized Al_2Cu-MOF/CF was employed as the working electrode, while a platinum wire served as the counter electrode as well as Ag/AgCl served as standard reference electrode. The M-OOHv (oxygen defect metal hydroxide) was electrochemically deposited on the surface of Al_2Cu-MOF using 10 CV cycles in the potential window (0 to 2 V) *vs.* Ag/AgCl inside 1 M aqueous solution of KOH at a sweeping speed of 5 mVs^{-1}. The deposited electrocatalyst (Al_2Cu-MOF@M-OOHv-ER/CF) was desiccated in electric oven at 60 °C.

2.4. Material characterization

The crystalline phases of different electrodes were investigated using an XRD (Advance D8 Bruker) with Cu Kα radiation and an accelerating potential of 40 kV in the 2θ range of 10–80°. Raman spectroscopy was used to analyze the material's phase change after it was manufactured (Alpha 300 R) under a He–Ne laser (excitation at 632 nm). The electrode surface morphologies were explored using SEM, and the elemental compositions of the electrodes were investigated using SEM-EDX (Quanta 200-FEG). FT-IR was recorded using a JASCO 6800 FTIR spectrometer with scans ranging from 4000 to 400 cm^{-1}. A Quantachrome Nova2200e BET surface area analyzer was utilized at 80 K to evaluate the specific surface areas.

2.5. Electrochemical measurement

The electrode material that was created acted as the functioning electrode, the counter electrode was made of a Pt wire and standard electrode was made of silver/silver chloride. This was all done in a Pyrex electrolytic cell with 1 M KOH as the electrolyte. An alkaline environment is generally utilized to analyze the O_2 evolution process because the O_2 evolution reaction includes the creation of defects after the OH^- loses electrons.

Using the Nernst equation, the potential values in this reading were translated into the RHE with the following eqn (1):[33]

$$E_{RHE} = E_{Ag/AgCl} + 0.059\ pH + E^{0}_{Ag/AgCl} \quad (1)$$

In the non-faradaic region in range of −0.2 V alongside 0.01 V (*vs.* RHE), electrode ECSAs were measured by cyclic voltammetry (CV) in a sweeping range of 10–50 mV s^{-1} (*vs.* RHE). The double-layer capacitance (C_{dl}) and ECSA were measured using the given expressions (2) and (3):[34,35]

$$C_{dl} = \frac{\text{Slope}}{2} \quad (2)$$

$$\text{ECSA} = \frac{C_{dl}}{C_{sp}} \quad (3)$$

Herein, C_{dl}, C_{sp} and ECSA are the double layer capacitance (mF), specific capacitance of the flat electrodes (NF, 0.04 mF cm^{-2}) and electrochemical active surface area (cm^2), respectively. By making a graph of the overpotential (η) *vs.* the current density, then Tafel slope was found. This Tafel slope gave information about the kinetic mechanism of the OER for the manufactured materials. Linear sweep voltammetry (LSV) with a 95% *iR* correction was used to get the OER polarization curves. The overpotential of the OER at 25 °C was computed with the given expression (3):[36]

$$\eta = E(\text{RHE}) - 1.23\ \text{V}. \quad (4)$$

With the use of the EIS approach, the OER mechanism has been further examined at frequencies ranging between 100 Hz and 100 kHz and an alternating current (AC) potential voltage around 5 mV at the open circuit voltage. The durability of the fabricated material in long-term was measured with chronoamperometry at the cell constant of 0.75 V.

3 Results and discussion

3.1. Structural, morphological, and textural characteristics

To investigate the physical features of the catalyst, the XRD patterns of Al_2Cu-MOF/CF and Al_2Cu-MOF@M-OOHv-ER/CF were explored in the 2θ range of 10 to 80°. The distinctive diffraction peaks detected in Al_2Cu-MOF/CF at 25.85°, 43.07°, and 53.16° correspond to the 002, 100, and 105 indexed planes, and other peaks located at 15.56° and 27.56° correspond to the 110 and 444 indexed planes, which were well consistent with the Al and Cu MOF as previously reported.[37,38] The existence of a bimetallic peak in Al_2Cu MOF indicates the successful fabrication of Al_2Cu MOF. Fig. 1 illustrates that the slight shifting in the 2θ value and variation in the peak intensity suggested the change in MOF phase to the metal hydroxy phase during the electro-oxidation reconstitution (ER). The absence of peaks at 60.29° and 62.82° in Al_2Co-MOF@MOOHv-ER/CF also confirms the phase transformation. Furthermore, phase transition and structure of the fabricated material were assessed with Raman spectroscopy as shown in Fig. 1(b). The presence of the characteristics peaks at 714.24, 925.42, 1181.21, 1452.23, and 1630.75 cm^{-1} is attributed to Al_2Cu-MOF/CF. The material

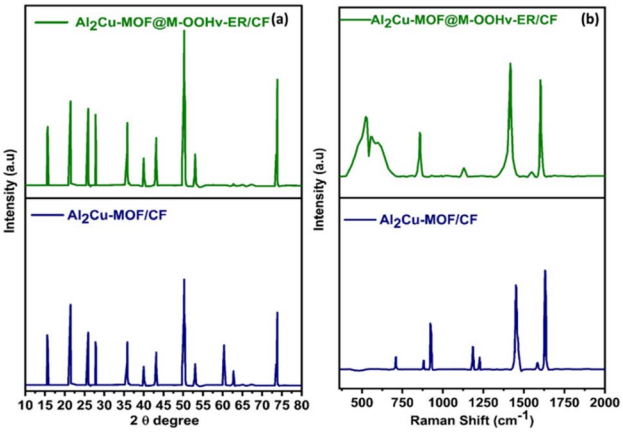

Fig. 1 (a) XRD diffractogram and (b) Raman spectroscopy of Al_2-CuMOF/CF and Al_2Cu-MOF@M-OOHv-ER/CF.

displays the characteristic peak of MOOH at 608 cm^{-1}.[47] The variation in peak intensity at 608 cm^{-1} and the production of MOOHv on the interface of Al_2Cu-MOF confirm the phase transition and oxygen defects that are present in the Al_2Cu MOF@M-OOHv-ER/CF.

Additionally, the molecular structural changes of Al_2Cu-MOF/CF and Al_2CuMOF@M-OOHv-ER/NF were determined with FT-IR as seen in Fig. 2(a). The stretching bands in Al_2Cu-MOF/NF and Al_2CuMOF@M-OOHv-ER/NF at 1610 cm^{-1} and 1390 cm^{-1} are due to vibrations that concerns carboxyl group from the ligand H_2BDC.[39,40] Additionally, the benzene ring's C–H bonding stretching from H_2BDC appeared at 780 cm^{-1}, and the other peaks located below 700 cm^{-1} are ascribed due to metal oxide (M–O) vibration modes in Al_2CuMOF/CF and Al_2Cu-MOF@M-OOHv-ER/CF.[41] The presence of FT-IR peaks demonstrates that Al_2CuMOF/CF, along with H_2BDC, was successfully developed.

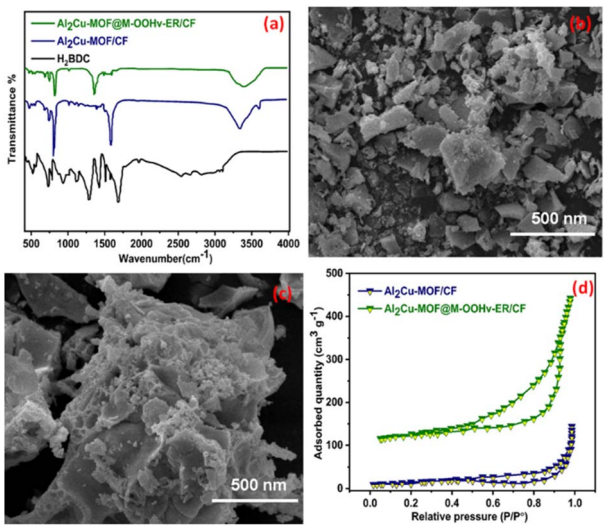

Fig. 2 (a) FTIR, (b and c) SEM micrograph and (d) textural properties of Al_2Cu-MOF/CF and Al_2Cu-MOF@M-OOHv-ER/CF.

Scanning electron microscopy (SEM) micrographs of Al_2-CuMOF/CF and Al_2Cu-MOF@M-OOHv-ER/CF are displayed at 500 nm in Fig. 2(b and c). The Al_2CuMOF/CF, which is composed of two-dimensional smooth irregular nanosheets, develops uniformly over the CF. Fig. 2(c) demonstrates that electro-oxidation reconstitution of the material results in a more abrasive and rougher Al_2Cu MOF surface, exposing more active edge sites for improving catalytic activity.[41,42] In addition, a rough surface implies the production of new compounds, which might reduce the effectiveness of catalysis. Fig. 2(d) illustrates the textural properties of the fabricated material measured under a nitrogen atmosphere at a comparative pressure (P/P_0) of 0 to 1.0. The BET isotherm displays the surface areas of Al_2CuMOF/CF and Al_2Cu-MOF@M-OOHv-ER/CF to be 68 and 173 $m^2\ g^{-1}$, respectively.[44–46] The BET result suggests that the high surface area of the bimetallic MOF increases the electrocatalytic efficiency of the material toward the OER activity.

3.2. Electrocatalytic OER performance

All OER activities regarding Al_2Cu-MOF/CF and Al_2Cu-MOF@M-OOHv-ER/CF were investigated in 1.0 M aqueous solution (KOH) configured with a three electrode system whose potential ranging from 0 to 2.0 V. Fig. 3(a) depicts about CV polarization curve of Al_2Cu-MOF@M-OOHv-ER/CF exhibited a higher current density than those of Al_2Cu-MOF/CF, RuO_2 and Cu foam.

Electro-oxidation reconstitution (Fig. 3(b)) showed the higher current density than Al_2Cu-MOF/CF, RuO_2 and Cu foam. Additionally, the Al_2Cu-MOF@M-OOHv-ER/CF nanostructured arrangements with a saw-tooth morphology may assist the uniformly dispersed M-OOHv in attaining the adsorption of OH ions at surface of the electrocatalyst that intensifies conductance of the material and exhibited OER's potent electrochemical performance.[43] LSV curves were used to calculate the Tafel slopes for each electrode, so that the whole electrode's OER reaction dynamics could be investigated more closely.

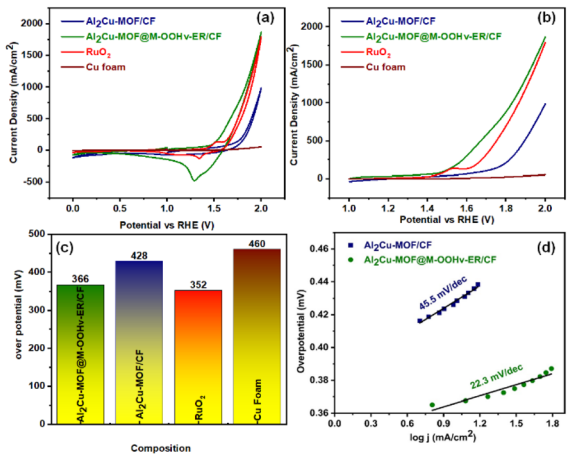

Fig. 3 (a) Cyclic voltammogram at various scanning rates, (b) LS voltammetry, (c) overpotential of Al_2Cu-MOF/CF, Al_2Cu MOF@M-OOHv-ER/CF, RuO_2 and Cu foam @ 10 mA cm^{-2} and (d) Tafel slope of Al_2Cu-MOF/CF and Al_2Cu-MOF@M-OOHv-ER/CF@ 10 mA cm^{-2}.

Furthermore, the Al_2Cu-MOF@M-OOHv-ER/CF (366 mV) delivers a better overpotential than Al_2Cu-MOF/CF (428 mV), RuO_2 (352 mV) and Cu foam (460 mV) as shown in Fig. 3(c). This may be the result of the M-OOHv adsorption at surface of Al_2Cu-MOF/CF.[44] For the kinetic mechanism the Tafel slope of Al_2Cu-MOF@M-OOHv-ER/CF had the lowest value (22.3 mV dec^{-1}) and delivered the fastest OER reaction kinetics than the other fabricated electrode as demonstrated in Fig. 3(d).

OER competence may also be investigated by calculating the electrochemical active surface area (ECSA) *via* using value of double layer capacitance (C_{dl}) with the help of eqn (2) and (3). Al_2Cu-MOF@M-OOHv-ER/CF exhibited the most exposed dynamic areas compared to the other fabricated electrode. The ECSA can be calculated using cyclic voltammograms at various scan rates as represented in Fig. 4(a and c). From these curves the C_{dl} values were calculated by plotting a graph between the change in current density and scan rate. All obtained C_{dl} results of Al_2Cu-MOF/CF and Al_2Cu-MOF@M-OOHv-ER/CF were 7.5 mF and 30.2 mF, respectively, as shown in Fig. 4(b and d). The ECSA results for Al_2Cu-MOF/CF and Al_2Cu-MOF@M-OOHv-ER/CF are 187.5 and 755.0 cm^2, respectively.

It is probable that the produced saw-tooth type of morphology of Al_2Cu-MOF@M-OOHv-ER/CF will exhibit the greatest ECSAs that will boost its OER electrochemical performance.[45]

For intrinsic activity, the ECSA normalized LSV curve is another way to evidence the remarkable OER activity of all prepared samples. The ECSA-normalized LSV curve is shown in Fig. 4(e). The obtained LSV curve for prepared samples has been normalized by ESCA 7.5 $m^2\ g^{-1}$ and 30.2 $m^2\ g^{-1}$ for Al_2Cu-MOF/CF and Al_2Cu-MOF@M-OOHv-ER/CF. The given graph exhibits a higher current density normalized by ECSA in the case of Al_2Cu-MOF@M-OOHv-ER/CF as compared to Al_2Cu-MOF/CF; therefore, the prepared OER electrocatalyst can be used for commercial and business applications.

To find out more about the OER kinetics, EIS of the fabricated electrode was conducted. The EIS was evaluated in 1.0 M KOH and its frequency ranges through 100 Hz to 100 KHz. Utilizing the Nyquist curves, we were able to determine the resistance values of all electrocatalysts. Compared to the Al_2Cu-MOF/CF (14 Ω), the Al_2Cu-MOF@M-OOHv-ER/CF electrode depicts extraordinarily low R_{ct} value of (5.7 Ω), which corresponds to the higher oxygen evolution efficiency and lower Tafel slope results. As a consequence, the Al_2Cu-MOF@M-OOHv-ER/CF exhibits strong catalytic activity, and good electron transfer capacity.[46–50]

In addition to electrocatalytic properties, the practical application of Al_2Cu-MOF@M-OOHv-ER/CF was determined through chronoamperometry. The Al_2Cu-MOF@M-OOHv-ER/CF operates for 50 h without experiencing considerable attenuation and has better stability than RuO_2 (Fig. 5(b)).

The structural durability of the Al_2Cu-MOF@M-OOHv-ER/CF was also determined with XRD analysis. The XRD structure stability result suggests that the electrocatalyst is stable over 50 hours, as shown in Fig. 5(c). Additionally, there was no discernible change between the CV curves before and after the durability test, demonstrating exceptional endurance of Al_2Cu MOF@M-OOHv-ER/CF, as shown in Fig. 5(c).

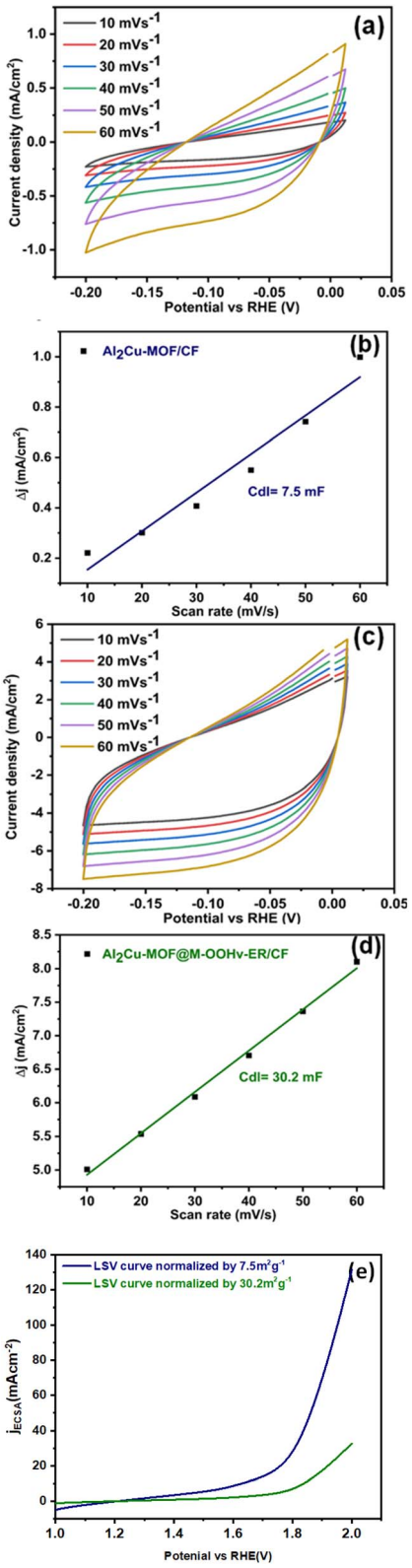

Fig. 4 (a and c) Cyclic voltammogram, (b and d) C_{dl} plot profile, and (e) normalized plot profile of Al_2Cu-MOF/CF and Al_2Cu-MOF@M-OOHv-ER/CF.

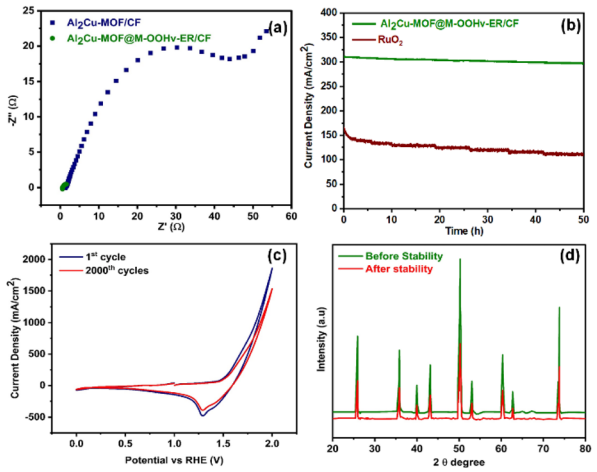

Fig. 5 (a) EIS of Al_2Cu-MOF/CF and Al_2Cu MOF@M-OOHv-ER/CF, (b) chronoamperometry of Al_2Cu MOF@M-OOHv-ER/CF and RuO_2, (c) XRD stability and (d) CV stability cycles of Al_2Cu-MOF@M-OOHv-ER/CF.

4 Conclusions

In conclusion, a novel technique has been created to transform Al_2Cu-MOF/CF into Al_2Cu-MOF@M-OOHv-ER/CF *via* electro-oxidation reconstitution that has many oxygen defects on the surface. When analysed with a three-electrode system under 1.0 M aqueous solution, and a current density of around 10 mA cm^{-2} Al_2Cu-MOF@M-OOHv-ER/CF showed lesser overpotential around 224 mV. The Al_2Cu-MOF@M-OOHv-ER/CF also displays minimal Tafel slope of 95.2 mV dec^{-1} having larger ECSA with a C_{dl} of 30.2 mF. *In situ* Raman spectroscopy discloses active sites for the OER when the MOF phase transforms into the MOOHv phase. Various analytical techniques of the structure determination helped in betterment of catalytic activity were responsible for the bimetal synergistic effect & oxygen defects in MOOHv, which affects electron density of states. The newly developed Al_2Cu-MOF@M-OOHv-ER/CF, which resembles a rough surface, can be produced using a quick, easy, and environmentally friendly process and has remarkable potential for O_2 evolution. The *in situ* electrooxidation reconstitution process proposed in this project offers a unique way to transform MOF materials into derivatives that are catalytically active.

Author contributions

All authors have equal contribution.

Conflicts of interest

There are no conflicts to declare.

Acknowledgements

The authors express their gratitude to Princess Nourah bint Abdulrahman University Researchers Supporting Project (Grant No. PNURSP2023R70), Princess Nourah bint Abdulrahman University, Riyadh, Saudi Arabia.

References

1 M. Hassan, Y. Slimani, M. A. Gondal, M. J. Mohamed, S. Güner, M. A. Almessiere and A. Trukhanov, *Ceram. Int.*, 2022, **48**, 24866–24876.
2 D. A. Vinnik, V. V. Kokovkin, V. V. Volchek, V. E. Zhivulin, P. A. Abramov, N. A. Cherkasova, Z. Sun, M. I. Sayyed, D. I. Tishkevich and A. V. Trukhanov, *Mater. Chem. Phys.*, 2021, **270**, 124818.
3 A. V. Trukhanov, V. O. Turchenko, I. A. Bobrikov, S. V. Trukhanov, I. S. Kazakevich and A. M. Balagurov, *J. Magn. Magn. Mater.*, 2015, **393**, 253–259.
4 M. Zdorovets, A. Kozlovskiy, D. Tishkevich, T. Zubar and A. Trukhanov, *J. Mater. Sci.: Mater. Electron.*, 2020, **31**, 21142–21153.
5 S. Manzoor, M. Sadaqat, S. J. H. hah, S. Gouadria, F. Hussain, K. S. Joya and M. N. Ashiq, *Fuel*, 2022, **319**, 123797.
6 X. Xu, R. Wang, S. Chen, A. Trukhanov, Y. Wu, L. Huang and Z. Sun, *Inorg. Chem. Front.*, 2022, **9**, 5507–5516.
7 S. Cao and J. Yu, *Chem. Lett.*, 2014, **5**, 2101–2107.
8 O. Polat and N. Sahiner, *Int. J. Energy Res.*, 2022, **46**, 14587–14608.
9 S. J. Mun and S. J. Park, *Catalysts*, 2019, **9**(10), 805.
10 M. S. Reza, N. B. H. Ahmad, S. Afroze, J. Taweekun, M. Sharifpur and A. K. Azad, *Chem. Eng. Technol.*, 2022, **46**(3), 420–434.
11 A. Naseri, A. M. Samadi, A. Pourjavadi, A. Z. Moshfegh and S. Ramakrishna, *J. Mater. Chem. A*, 2017, **5**, 23406–23433.
12 Z. Chen, L. Guo, L. Pan, T. Yan, Z. He, Y. Li, C. Shi, Z. Huang, X. Zhang and J. Zou, *Adv. Energy Mater.*, 2022, **12**, 2103670.
13 Y. Gao, D. Kong, F. Cao, S. Teng, T. Liang, B. Luo, B. Wang, Q.-H. Yang and L. Zhi, *Nano Res.*, 2022, **15**, 7959–7967.
14 N. Prabu, R. S. A. Saravanan, T. Kesavan, G. Maduraiveeran and M. Sasidhara, *Carbon*, 2019, **152**, 188–197.
15 Y. Zhu, T. R. Kuo, Y. H. Li, M. Y. Qi, G. Chen, J. Wang, Y. J. Xu and H. M. Chen, *Energy Environ. Sci.*, 2021, **14**, 1928–1958.
16 A. V. Trukhanov, V. G. Kostishyn, L. V. Panina, V. V. Korovushkin, V. A. Turchenko, P. Thakur, A. Thakur, Y. Yang, D. A. Vinnik, E. S. Yakovenko, L. Y. Matzui, E. L. Trukhanova and S. V. Trukhanov, *J. Alloys Compd.*, 2018, **754**, 247–256.
17 S. V. Trukhanov, A. V. Trukhanov, V. A. Turchenko, E. L. Trukhanova, D. I. Tishkevich, V. M. Ivanov, T. I. Zubar, M. Salem, V. G. Kostishyn, L. V. Panina, D. A. Vinnik and S. A. Gudkova, *Ceram. Int.*, 2018, **44**, 290–300.
18 M. A. Almessiere, A. V. Trukhanov, Y. Slimani, K. Y. You, S. V. Trukhanov, E. L. Trukhanova, F. Esa, A. Sadaqati, K. Chaudhary, M. Zdorovets and A. Baykal, *Nanomaterials*, 2019, **9**, 202, DOI: **10.3390/nano9020202**.
19 J. Zhu, B. Zeng, L. Mo, F. Jin, M. Deng and Q. Zhang, *Appl. Clay Sci.*, 2021, **206**, 106070.
20 S. Fu, C. Zhu, J. Song, D. Du and Y. Lin, *Adv. Energy Mater.*, 2017, **7**, 1700363.
21 Q. Qian, Y. Li, Y. Liu, L. Yu and G. Zhang, *Adv. Mater.*, 2019, **31**, 1901139.
22 Y. Yang, Y. Yang, Y. Liu, S. Zhao and Z. Tang, *Small Sci.*, 2021, **1**, 2100015.
23 N. Cheng, L. Ren, X. Xu, Y. Du and S. X. Dou, *Adv. Energy Mater.*, 2018, **8**, 1801257.
24 D. Wang, D. Y. Jana and Y. Zhao, *Acc. Chem. Res.*, 2020, **53**, 1389–1400.
25 A. Indra, T. Song and U. Paik, *Adv. Mater.*, 2018, **30**, 1705146.
26 T. Montini, M. Melchionna, M. P. Monai and P. Fornasiero, *Chem. Rev.*, 2016, **116**, 5987–6041.
27 Y. Li, Z. Y. Fu and B. L. Su, *Adv. Funct. Mater.*, 2012, **22**, 4634–4667.
28 A. Trovarelli, *Catal. Rev. - Sci. Eng.*, 1996, **38**, 439–520.
29 Z. Gao, Z. W. Yu, F. Q. Liu, C. Yang, Y. H. Yuan and Yu F. Luo, *ChemSusChem*, 2019, **12**, 4623–4628.
30 S. Niu, C. Li, J. Huo, W. Dong, S. El Hankari, Y. Liang and Q. Li, *ACS Omega*, 2021, **6**, 13946–13952.
31 X. Ling, F. Du, Y. Zhang, Y. Shen, W. Gao, B. Zhou, Z. Wang, G. Li, T. Li, Q. Shen, Y. Xiong, X. Wang, Y. Zhou and Z. Zou, *J. Mater. Chem. A*, 2021, **9**, 13271–13278.
32 F. Liu, W. Jin, Y. Li, L. Zheng, Y. Hu, X. Xu, Y. Xue, C. Tang, H. Liu and J. Zhang, *Appl. Surf. Sci.*, 2020, **529**, 147125.
33 D. Chu and J. Li, *ECS Trans.*, 2020, **97**, 575–580.
34 L. Zhang, H. Jang, H. Liu, M. G. Kim, D. Yang, X. Liu, S. Liu and J. Cho, *Angew. Chem., Int. Ed.*, 2021, **60**, 18821–18829.
35 W. Cheng, Z. P. Wu, D. Luan, S. Q. Zang and X. W. Lou, *Angew. Chem., Int. Ed.*, 2021, **60**, 26397–26402.
36 J. Seong Kim, I. Park, E.-S. Jeong, K. Jin, W. Mo Seong, G. Yoon, H. Kim, B. Kim, K. Tae Nam, K. Kang, J. S. Kim, I. Park, E. Jeong, K. Jin, W. M. Seong, G. Yoon, H. Kim, B. Kim, K. T. Nam and K. Kang, *Adv. Mater.*, 2017, **29**, 1606893.
37 R. Nivetha, A. Sajeev, A. Mary Paul, K. Gothandapani, S. Gnanasekar, G. Jacob, R. Sellappan, V. Raghavan, N. Krishna Chandar, S. Pitchaimuthu, S. K. Jeong and A. Nirmala Grace, *Mater. Res. Express*, 2020, **7**, 114001.
38 X. Zeng, J. Wenwu, H. Li, I. Saikumar and Q. Zhang, *Nanotechnology*, 2022, **31**, 1–22.
39 H. Ren, T. Y. Song, J. N. Xu, S. B. Jing, Y. Yu, P. Zhang and L. R. Zhang, *Cryst. Growth Des.*, 2009, **9**, 105–112.
40 M. M. Jia, X. Y. Zhang, Q. L. Yang, D. Q. Xiong, P. K. Fu, M. M. Jiao, X. L. Wang and X. Y. Dong, *J. Coord. Chem.*, 2021, **74**, 2641–2656.
41 H. P. Nguyen Thi, H. D. Ninh, C. Van Tran, B. T. Le, S. V. Bhosale and D. D. La, *ChemistrySelect*, 2019, **4**, 2333–2338.
42 C. H. Choi, S. H. Park and S. I. Woo, *ACS Nano*, 2012, **6**, 7084–7091.
43 Y. Zhang, J. Wang, L. Ye, M. Zhang and Y. Gong, *Dalton Trans.*, 2021, **50**, 4720–4726.
44 M. Vandichel, K. Laasonen and I. Kondov, *Top. Catal.*, 2020, **63**, 833–845.
45 Y. Chen, Z. Yu, R. Jiang, J. Huang, Y. Hou, J. Chen, Y. Zhang, H. Zhu, B. Wang and M. Wang, *Small*, 2021, **17**, 2101003.
46 H. He, Y. Wang, J. Li, S. Jiang, S. Sidra, W. Gong, Y. Tang, Y. Hu, R. Wei, D. Yang, X. Li and Z. Zhao, *Chem. Eng. J.*, 2022, **427**, 131962.

47 N. Ma, J. Xu, Z. Bian, Y. Yang, L. Zhang and H. Wang, *Chem. Eng. J.*, 2020, **389**, 123426.
48 T. I. Zubar, V. M. Fedosyuk, A. V. Trukhanov, N. N. Kovaleva, K. A. Astapovich, D. A. Vinnik, E. L. Trukhanova, A. L. Kozlovskiy, M. V. Zdorovets, A. A. Solobai, D. I. Tishkevich and S. V. Trukhanov, *J. Electrochem. Soc.*, 2019, **166**, D173–D180.
49 T. Zubar, V. Fedosyuk, D. Tishkevich, O. Kanafyev, K. Astapovich, A. Kozlovskiy, M. Zdorovets, D. Vinnik, S. Gudkova, E. Kaniukov, A. S. B. Sombra, D. Zhou, R. B. Jotania, C. Singh, S. Trukhanov and A. Trukhanov, *Nanomaterials*, 2020, **10**, 1–14.
50 M. Chen, G. C. Wang, W. Q. Yang, Z. Y. Yuan, X. Qian, J. Q. Xu, Z. Y. Huang and A. X. Ding, *ACS Appl. Mater. Interfaces*, 2019, **11**, 42156–42171.